To the Graduate Council:

I am submitting herewith a thesis written by Charles Martin entitled "Low Energy Electron Attenuation Lengths in Thin Amorphous Carbon Films." I have examined the final copy of this thesis for form and content and recommend that it be accepted in partial fulfillment of the requirements for the degree of Master of Science, with a major in Physics.

T. A. Callcott

T. A. Callcott, Major Professor

We have read this thesis and recommend its acceptance:

James A. Ferrell

Harold C. Schweinler

Accepted for the Council:

Lew Minkel

Vice Chancellor
Graduate Studies and Research

LOW ENERGY ELECTRON ATTENUATION LENGTHS IN THIN AMORPHOUS CARBON FILMS

A Thesis

Presented for the

Master of Science

Degree

The University of Tennessee, Knoxville

Charles Martin

August 1983

DEDICATION

This thesis is dedicated to my parents, Dr. C. M. Blood and Mrs. W. P. Martin, of Cleveland, Tennessee, for their sincere encouragement, and to my life partner and my best friend, Jo Anna Hickman, for living the existential crisis and for (temporarily) saving me from the excruciating life of tournament chess.

ACKNOWLEDGMENTS

The author wishes to express his gratitude to Dr. T. A. Callcott and Dr. E. T. Arakawa for the thoughtful leadership and considerable time spent during the course of this research. Appreciation is extended to the Oak Ridge National Laboratory for allowing the author to use the research facilities of the Biological and Radiation Physics Section of the Health and Safety Research Division and for financial support provided by the U. S. Department of Energy under Contract No. W-7405-eng-26 with the Union Carbide Corporation. Special thanks go to Maxine Martin for the typing of this manuscript.

The author wishes to express his appreciation for the classroom guidance of Dr. R. D. Present whose courses at The University of Tennessee, Knoxville have made my undergraduate and graduate education meaningful.

ABSTRACT

The results of energy loss experiments on low energy electrons passing through thin amorphous carbon films are reported. For electron energies between 50 and 3000 eV, electron attenuation lengths were determined by electron transmission measurements through carbon films of thicknesses between 81 and 210 Å. The density of amorphous carbon was also obtained by a sink-float method and found to be 1.90 ± 0.05 g/cm^3. The electron attenuation length was found to increase monotonically from approximately 12 to 58 Å over the 50 to 3000 eV energy range. Over the 500 to 3000 eV energy region, the results are in good agreement with the theoretical predictions for amorphous carbon with the same density.

TABLE OF CONTENTS

LIST OF FIGURES

CHAPTER I

INTRODUCTION

Information about electron attenuation in solids is important for a wide variety of applications. In the past most experimental investigations have used electrons with energies greater than about 10 keV. The region of lower energy is experimentally difficult because electron penetration is too weak to allow measurable transmission through metal films of more than a few hundred angstroms thickness. Since thinner films are difficult to prepare, there is virtually no experimental data in the low energy region. This thesis describes an experimental investigation of the interesting region of low energy and reports values of the electron attenuation length for energies between 50 and 3000 eV.

There have been two major types of experimental studies of electron energy losses. One type studies the energy losses of electrons reflected from a target surface, and the other examines energy losses of electrons transmitted through thin films. In 1930 Rudberg[1] first studied energy losses of electrons reflected from thin metal films and observed the energy loss peaks of the reflected electron beam. In 1941, Ruthemann[2] made the first observations of energy losses of fast electrons passing through a thin metal foil. In order to observe any transmission through the foil, he had to use electrons in the kilovolt region. Since this early work, there have been many investigations of both types employing a wide variety of experimental techniques.[3]

Since one has no way of accurately measuring the distance that an electron travels into the target in reflection measurements, the transmission method is much more suitable for the determination of electron attenuation lengths. A measurement of the fraction of electrons penetrating the foil without energy loss or angular deflection gives a direct measure of the electron scattering length.

In 1951 Bohm and Pines[4] proposed that energetic electrons lose energy in a solid by exciting density oscillations in the electron gas at a characteristic plasma frequency. When they applied this theory to the conduction electrons of metals, they found that the energy loss of an energetic electron was

$$\hbar\omega_p = \hbar\left(\frac{4\pi ne^2}{m}\right)^{1/2} \tag{1}$$

where ω_p is the bulk plasmon frequency, n is the number density of free electrons in the metal, and e and m are the charge and mass, respectively, of the electron. These are the so-called volume plasmon excitations.

In studying the interaction of fast electrons with the conduction electrons of a metal foil in contact with a vacuum, a reduced energy loss of $\frac{\hbar\omega_p}{\sqrt{2}}$ was predicted by Ritchie[5] in 1957 for the excitation of surface density oscillations, or surface plasmons at a thick film-vacuum interface. If the film had a spherical grain, the result would be lowered to $\frac{\hbar\omega_p}{\sqrt{3}}$. Ritchie also derived a dispersion relation for surface plasmons on a thin metal foil where the interference effects couple the oscillations on the two foil surfaces. The result was

$$\omega_s = \frac{\omega_p}{\sqrt{2}} [1 \pm \exp(-ak)]^{1/2} , \qquad (2)$$

where a is the foil thickness and k is the wave-vector of the surface plasmon wave.

In 1960 Stern and Ferrell[6] extended Ritchie's result showing that the frequency should be $\frac{\omega_p}{(1 + \varepsilon)^{1/2}}$ where ε is the dielectric constant of the medium surrounding the metal. For a metal under vacuum ($\varepsilon = 1$), this reduces to Ritchie's result.

In 1962 Quinn[7] used a self-energy approach to derive an expression for the mean free path of an energetic electron creating volume plasmons. He expressed the mean free path, λ, as

$$\lambda = \frac{2a_o E}{\hbar\omega_p} \left[\ell n \left\{ \frac{(p_o^2 + 2m\hbar\omega_p)^{1/2} - p_o}{p - (p^2 - 2m\hbar\omega_p)^{1/2}} \right\} \right]^{-1} \qquad (3)$$

where a_o is the Bohr radius, E is the electron energy, p_o is the electron momentum at the Fermi level, m is the mass of the electron, and p is the electron momentum. Plotting λ as a function of the incident electron energy, $E = p^2/2m$, we get the curve in Figure 1.

Early experimental findings by Blackstock et al.[8] (1955), Jull[9] (1956), and others seemed to verify the theory at high energies although the experimental errors were rather high. These experiments involved shooting high energy electrons through metallic films with thicknesses between 200 to 1000 Å. No data, however, were reported below 10 keV because of the difficulty of making sufficiently thin continuous, free-standing films for electron transmission.

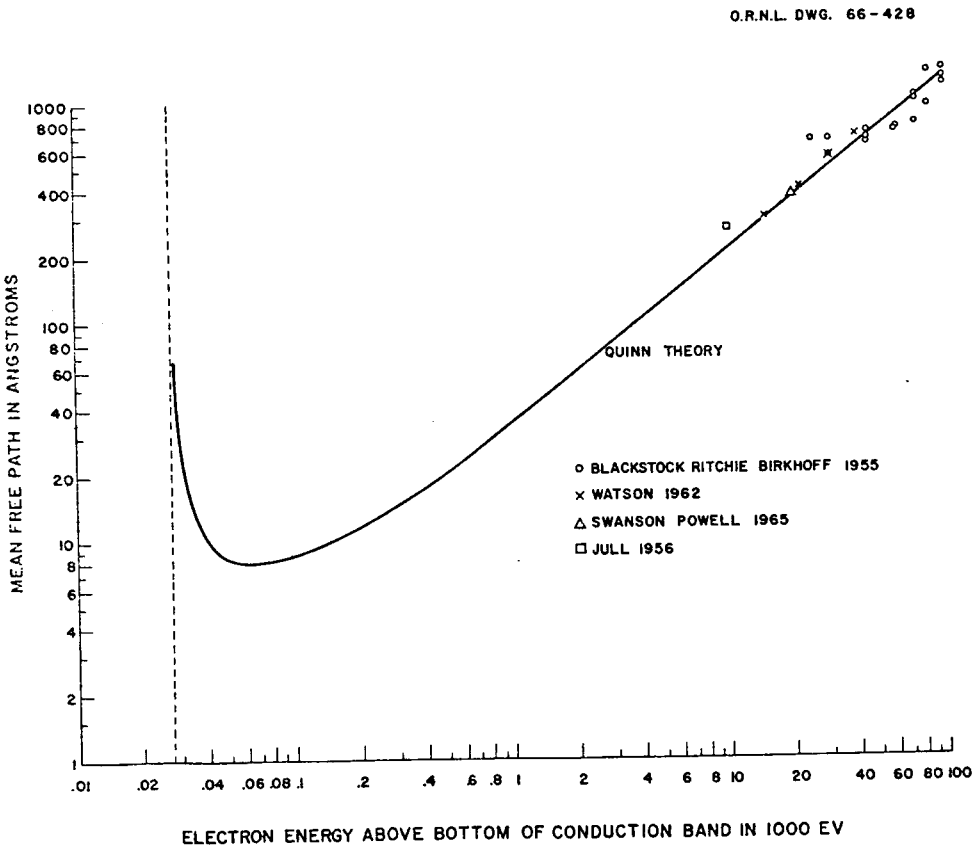

Figure 1. Electron mean free path for plasmon creation as a function of electron energy. The Quinn theory is the solid curve; various experimental data are shown as points.

Other workers such as Crowell et al.[10] (1962), Soshea and Lucas[11] (1965), and Garber et al.[12] (1969) used photoemission techniques on a metal-oxide-metal sample or on a thin metal foil evaporated onto a semiconductor. By measuring the number of photoelectrons collected in the oxide layer or semiconductor per absorbed photon, the attenuation length of hot electrons could be found as a function of sample thickness. This method requires the use of optical constants of the metal under study in calculating the electron attenuation length, and has the disadvantage that electron transmission cannot be directly measured. Widely varying results were reported by different experimental groups depending on which set of optical constants were used in the analysis.

Due to the lack of experimental transmission data in the low energy region (50 to 3000 eV), it was decided that this would be a good area of investigation. The chief experimental problem was to obtain uniform and continuous free-standing thin films. Amorphous carbon was chosen because a great deal was known about its electrical and optical properties, and the manufacture of thin free-standing films appeared promising. Carbon films are strong and have uniform cross sections even when very thin. Metal films, in contrast, are often brittle and tend to form island and network structures when very thin. Because published values[13] of the density of amorphous carbon vary widely depending upon the procedure used in obtaining them, it was also necessary to devise a way to accurately determine the density of the particular films studied.

The purpose of this study then was to obtain data on the interactions of low energy electrons passing through thin amorphous

carbon films under high vacuum conditions in order to calculate the electron attenuation length for a known film density. A state-of-the-art method for manufacturing thin amorphous carbon films is also presented.

CHAPTER II

THEORY

Basic Assumptions

The theory of electron transmission through thin films involves examining the energy loss mechanisms of the electron. The dominant interactions are elastic scattering, inelastic electron-valence electron scattering, inner shell electron ionizations, inelastic electron-surface plasmon excitations, and inelastic electron-volume plasmon excitations.

Elastic scattering results from electrons colliding elastically with the lattice without appreciable loss of energy. The encounters result in a new path direction for the electron in the lattice. Upon leaving the sample, purely elastically scattered electrons are scattered in angle, but not reduced in energy. At sufficiently high energies, elastic scattering of electrons can be regarded as screened Rutherford scattering; energetic electrons are scattered from individual ions in the lattice. This process involves no coherent scattering.

Inelastic collisions of electrons with electrons in the conduction band can result in significant energy losses. These electron-electron collisions may be calculated using an electron gas model of the conduction band, and will result in the generation of secondary electrons. Electron-valence electron interactions are usually treated in the free electron gas approximation ignoring interband matrix elements. Core electrons, like valence electrons, may be excited in electron-electron

collisions when the electron energy is greater than twice the core binding energy. For amorphous carbon, core interactions occur at energies above 560 eV, but provide small contributions to the mean free path calculations.

Plasmon excitations result in significant energy losses above the plasma frequency. Surface plasmons are created by an energetic electron passing through the surface, and later decay by creating an electron-hole pair in the conduction band. Volume plasmons are produced in the interior of the film and decay by interactions with the conduction band electrons. As mentioned earlier, in 1962 Quinn derived an expression for the mean free path for plasmon excitation which can be expressed as

$$\lambda_p(E) = \frac{2a_o E}{\hbar\omega_p} \left(\ell n \left(\frac{\sqrt{E_o + \hbar\omega_p} - \sqrt{E_o}}{\sqrt{E} - \sqrt{E - \hbar\omega_p}} \right) \right)^{-1} \qquad (4)$$

where:

E_o is the Fermi energy in the metal;

E is the incident energy of the electron;

$\hbar\omega_p$ is the plasma energy of the target;

a_o is the Bohr radius.

The equation applies only when $E>(E_o+\hbar\omega_p)$; at energies below the plasma energy, electron excitation will not produce a plasmon. At the low energies just above the plasma energy, plasmon excitation is the dominant inelastic scattering mechanism. As was shown in Figure 1, this contribution to the mean free path passes through a minimum for electron energies between 40 and 100 eV and rises monotonically at higher energies. Several compilations of mean free path data are available in the literature.[14]

MFP Theories Using the Dielectric Function

The response of any uniform medium to an electric field may be expressed in terms of $\varepsilon^*(\bar{k},\omega)$, the frequency and wavevector dependent complex dielectric function. The real part of this function, $\varepsilon_1(\bar{k},\omega)$, is a measure of the polarization response of the medium, and the imaginary part, $\varepsilon_2(\bar{k},\omega)$, is a measure of energy absorption. A standard result of theory is that the energy losses of a charged particle moving in a dielectric medium is proportional to the energy loss function, $\mathrm{Im}[\frac{-1}{\varepsilon^*(\bar{k},\omega)}]$.

The derivation begins by considering a nonrelativistic charged particle travelling with velocity v through a frequency dependent dielectric, $\varepsilon(\omega)$. It is assumed that the ion has no recoil, and only the longitudinal component of the dielectric function is considered. Poisson's equation states:

$$\varepsilon(\omega)\nabla^2\phi = -4\pi Ze\delta^3(\bar{r} - \bar{v}t) \ . \tag{5}$$

Substituting a potential ϕ of the form

$$\phi(\bar{r},t) = \frac{1}{(2\pi)^4} \iiint d^3k \int d\omega \ e^{i(\bar{k}\cdot\bar{r}-\omega t)}\phi_{\bar{k},\omega} \tag{6}$$

gives

$$\phi_{\bar{k},\omega} = \frac{8\pi^2 Ze\delta(\omega - \bar{k}\cdot\bar{v})}{\varepsilon(\omega)k^2} \ . \tag{7}$$

The potential and corresponding electric field, $\bar{E} = -\nabla\phi$, become

$$\phi(\bar{r},t) = \frac{Ze}{2\pi^2}\iiint \frac{d^3k}{k^2}\int d\omega\ \frac{e^{i(\bar{k}\cdot\bar{r}-\omega t)}\delta(\omega-\bar{k}\cdot\bar{v})}{\varepsilon(\omega)} \tag{8}$$

$$\bar{E}(\bar{r},t) = -\frac{Ze}{2\pi^2}\iiint \frac{d^3k}{k^2}\int d\omega(i\bar{k})\ \frac{e^{i(\bar{k}\cdot\bar{r}-\omega t)}\delta(\omega-\bar{k}\cdot\bar{v})}{\varepsilon(\omega)} \tag{9}$$

Generalizing $\varepsilon(\omega)$ over momentum space, let

$$\varepsilon(\omega) \rightarrow \varepsilon(\bar{k},\omega)\ .^{15} \tag{10}$$

Since only the electric field in the medium is desired, it is necessary to subtract the "bare" (or external) field. For a particle travelling in the z-direction, the potential $\phi_m(\bar{r},t=\frac{z}{v})$ and electric field $E_m(\bar{r},t=\frac{z}{v})$ in the medium are then

$$\phi_m(\bar{z},v) = \frac{Ze}{2\pi^2}\iiint \frac{d^3k}{k^2}\int d\omega\ e^{i(\bar{k}\cdot\bar{z}-\frac{\omega z}{v})}\delta(\omega-\bar{k}\cdot\bar{v})[\frac{1}{\varepsilon(\bar{k},\omega)}-1]\ , \tag{11}$$

and

$$E_m(\bar{z},v) = -\nabla\phi_m(\bar{z},v) = -\frac{Ze}{2\pi^2}\iiint \frac{d^3k}{k^2}\int d\omega(i\bar{k})e^{i(\bar{k}\cdot\bar{z}-\frac{\omega z}{v})}\delta(\omega-\bar{k}\cdot\bar{v})[\frac{1}{\varepsilon(\bar{k},\omega)}-1]\ . \tag{12}$$

where

$$\begin{aligned} \bar{r} &= \bar{v}t\ , \\ x &= y = 0\ , \\ t &= \frac{z}{v}\ . \end{aligned} \tag{13}$$

The retarding force on a charged particle with charge Ze is then defined as

$$F_{ret} = -\frac{dE}{dz} = -Ze\bar{E}_m(\bar{z},v)$$

$$= \frac{Z^2e^2}{2\pi^2}\iiint \frac{d^3k}{k^2}\int d\omega\ (\frac{i\ \bar{k}\cdot\bar{v}}{v})e^{i(\bar{k}\cdot\bar{v}-\omega)}\delta(\omega-\bar{k}\cdot\bar{v})[\frac{1}{\varepsilon(\bar{k},\omega)}] - 1]. \quad (14)$$

To evaluate this integral, we divide the volume element d^3k into two parts, $d^2\kappa$ and $d\omega$, where

$$\omega = \bar{k}\cdot\bar{v} = k_z v\ , \quad (15)$$

$$k^2 = k_x^2 + k_y^2 + k_z^2 = \kappa^2 + (\frac{\omega}{v})^2\ , \quad (16)$$

$$d^3k = d^2\kappa dk_z = d^2\kappa\ \frac{d\omega}{v}\ . \quad (17)$$

Substituting, rearranging, and using the properties of the delta function gives

$$-\frac{dE}{dz} = \frac{Z^2e^2i}{2\pi^2v^2}\iint d^2\kappa \int_{-\infty}^{\infty} d\omega\left(\frac{\omega}{\kappa^2 + (\frac{\omega}{v})^2}\right)\left(\frac{1}{\varepsilon(\bar{k},\omega)} - 1\right)\ . \quad (18)$$

Using two Fourier lemmas

$$(i)\quad \varepsilon(\bar{k},-\omega) = \varepsilon^*(k,\omega) \quad (19)$$

$$(ii)\quad \int_{-\infty}^{\infty} g(\omega)d\omega = 2\ \mathrm{Re}\int_0^{\infty} g(\omega)d\omega\ , \quad (20)$$

and transforming to cylindrical coordinates gives

$$-\frac{dE}{dz} = \frac{2Z^2e^2}{2\pi^2v^2}\int 2\pi\kappa\ d\kappa \int_0^{\infty} d\omega\ \left(\frac{\omega}{\kappa^2 + (\frac{\omega}{v})^2}\right)\mathrm{Re}\{i[\frac{1}{\varepsilon^*(\bar{k},\omega)} - 1]\}$$

$$= \frac{2Z^2e^2}{\pi\hbar v^2}\int kdk \int_0^{\infty} d\omega\ \left(\frac{\hbar\omega}{k^2 + (\frac{\omega}{v})^2}\right)\ \mathrm{Im}\ [\frac{-1}{\varepsilon^*(\bar{k},\omega)}] \quad (21)$$

Since the charged particle travels with velocity v, the only accessible region of integration is over

$$\frac{\omega}{v} \leq k < \infty \quad , \quad 0 \leq \omega < \infty \ ,$$

or

$$0 \leq k < \infty \quad , \quad 0 \leq \omega \leq kv \ .$$

Thus,

$$-\frac{dE}{dz} = \frac{2Z^2e^2}{\pi\hbar v^2} \int_{k=\frac{\omega}{v}}^{\infty} \frac{dk}{k} \int_{\omega=0}^{\infty} d\omega \ \hbar\omega \ \mathrm{Im}\left[\frac{-1}{\varepsilon^*(k,\omega)}\right]$$

$$= \frac{2Z^2e^2}{\pi\hbar v^2} \int_{k=0}^{\infty} \frac{dk}{k} \int_{\omega=0}^{vk} d\omega \ \hbar\omega \ \mathrm{Im}\left[\frac{-1}{\varepsilon^*(k,\omega)}\right] \ . \qquad (22)$$

This is the result of the classical derivation of $-\frac{dE}{dz}$ for a charged particle passing through a dielectric medium using Poisson's equation. If Equation (22) is divided by energy $\hbar\omega$, we obtain the total probability per unit length that the ion will lose energy $\hbar\omega$ (or momentum $\hbar k$). This quantity is defined as the inverse mean free path, λ^{-1}.

$$\lambda^{-1}(v) = \frac{2Z^2e^2}{\pi\hbar v^2} \int_{k=\frac{\omega}{v}}^{\infty} \frac{dk}{k} \int_{\omega=0}^{\infty} d\omega \ \mathrm{Im}\left[\frac{-1}{\varepsilon^*(k,\omega)}\right] \ . \qquad (23)$$

This can be expressed in differential form as

$$\frac{d\lambda^{-1}}{d\omega} = \frac{2Z^2e^2}{\pi\hbar v^2} \int_{k=\frac{\omega}{v}}^{\infty} \frac{dk}{k} \ \mathrm{Im}\left[\frac{-1}{\varepsilon^*(k,\omega)}\right] \ . \qquad (24)$$

In the case of a fast electron, we convert to atomic units. The general expression for the differential inverse mean free path (DIMFP) for inelastic electron collisions becomes

$$\frac{d\lambda^{-1}}{d\omega} = \frac{1}{\pi E}\int_{q^-}^{q^+}\frac{dq}{q}\ \mathrm{Im}\left[\frac{-1}{\varepsilon^*(\bar{q},\omega)}\right] , \tag{25}$$

where:

$\hbar = m = e = Z = 1$ (using atomic units),

$E = \frac{v^2}{2}$ is the energy of the electron,

v is the velocity of the electron,

$q = k$ is the momentum transfer,

ω is the plasma frequency of the sample,

$q^{\pm} = v \pm (v^2 - 2\omega)^{1/2}$ are the limits on integration, and

$\mathrm{Im}\left[\frac{-1}{\varepsilon^*(\bar{q},\omega)}\right]$ is called the energy loss function for volume plasmons. Similarly, the inverse mean free path (IMFP), λ^{-1}, is obtained from an integration over ω. In atomic units it is

$$\lambda^{-1} = \frac{1}{\pi E}\int_{q^-}^{q^+}\frac{dq}{q}\int d\omega\ \mathrm{Im}\left[\frac{-1}{\varepsilon^*(\bar{q},\omega)}\right] . \tag{26}$$

Various published calculations of λ^{-1} differ in the assumption made in the evaluation of this integral.

D. R. Penn[16] used the dielectric function of a free electron gas and calculated the λ^{-1} integral based on a model calculation of energy losses. For any pure material he found an expression,

$$\lambda = \frac{E}{a(\ell nE + b)} , \tag{27}$$

for the total mean free path derived from the electron concentration for each material. The quantities a and b depend on the dielectric function, $\varepsilon(\bar{q},\omega)$, which is not well known a priori for nonfree electron-like materials. He argued that an expression of this form should be valid for all materials depending on the specific form of $\varepsilon(\bar{q},\omega)$. He suggested further that most materials approximate a free electron gas when interacting with electrons of sufficiently high energy, and published values of λ calculated using this assumption, The equation does not hold for energies below 200 eV.

J. C. Ashley and M. W. Williams[17] have calculated λ from values of $\mathrm{Im}[\frac{-1}{\varepsilon^*(0,\omega)}]$ derived from optical data. In the calculation they assumed a model function of the form

$$\mathrm{Im}\left[\frac{-1}{\varepsilon^*(\bar{q},\omega)}\right] = \begin{cases} \sum_i \dfrac{A_i \gamma_i \omega}{\left(\omega^2 - \left[\omega_{oi} + \frac{q^2}{2}\right]^2\right)^2 + (\gamma_i \omega)^2}, & \omega > \omega_c \\ 0, & \omega < \omega_c \end{cases} \quad (28)$$

where ω_c is the cutoff frequency of the solid. This function was fit to optical data in the limit $q \to 0$ to determine values for the constants A_i, γ_i, ω_{oi}. The loss function was then extended to finite q by replacing ω_{oi} by $(\omega_{oi} + \frac{q^2}{2})$ as discussed in Ref. 17. This extension simply adds a free electron-like kinetic energy term which is associated with momentum transfer in the collision. Thus, Ashley's method assumes a free electron behavior in the extension from zero to finite momentum transfer, but not in the determination of the zero momentum energy loss spectrum, $\mathrm{Im}[\frac{-1}{\varepsilon^*(0,\omega)}]$. When applied to a free electron dielectric

function, the calculation gives results nearly identical to those of Penn, but when applied to other energy loss spectra, the results can be very different.

Using this method, Ashley and Williams calculated the inverse mean free paths for several organic insulators using optical data. For the materials tested, they found a mean free path of the form,

$$\lambda(E) = \frac{E}{A \ln E + B + \frac{C}{E}} \tag{29}$$

where A, B, and C are linear functions of n_v, the valence electron density, and λ is a function of the electron energy E. For a proper choice of constants, the electron density in atomic units can be expressed in terms of the volume density of the material, ρ, as

$$n_v = \frac{\rho n_{ve}}{M} \tag{30}$$

where

M = 12.001 g/g-mole is the molecular weight of carbon,

n_{ve} = 4 is the number of valence electrons for carbon.

Finally, the electron mean free path can be expressed as

$$\lambda(E) = \frac{0.75E}{\rho}\left(13.6 \ln E - 17.6 - \frac{1400}{E}\right)^{-1}, \tag{31}$$

where E is expressed in eV, λ is in $\mathring{A}$, and ρ = 1.90 g/cm^3 for amorphous carbon. Except for the dependence on ρ, this is a "universal energy loss curve." It is of interest to note that λ is proportional to the inverse of the volume density, $\lambda \propto \frac{1}{\rho}$. Equation (31)

is an empirical equation valid over the energy range from 200 eV to 10 keV, and breaks down for incident electron energies below 200 eV. Contributions due to the core electrons has a similar equation, but they have been neglected because they are small over this energy range.

For these organic solids then, the valence electron concentration n_v, is the only adjustable parameter in this theory. Since amorphous carbon and organic insulators have similar electron densities and plasma frequencies, we wished to see if our data fit with the "universal curve."

It is clear that the best procedure would be to compare our results to the inelastic mean free paths calculated using an energy loss function derived from optical measurements on our amorphous carbon films. Unfortunately, the properties of amorphous carbon are not well defined, but depend strongly on the method of preparation. Different preparation methods produce material of widely different properties.

Properties of Amorphous Carbon

In considering the attenuation length of electrons in amorphous carbon, it is necessary to consider the properties of the sample. For electron energies much larger than the typical bandwidth energy, losses may be approximately modeled using a free electron gas. In this model carbon differs from metals primarily by having a higher plasma frequency. In carbon $\hbar\omega_p$ is about 20 eV rather than the 5 to 10 eV typical of most metals. Interband matrix elements may also have

to be taken into account when considering low energies, but will not be explicitly considered here.

A solid is said to be amorphous when it lacks long range order though short range order may still be present. The ordered forms of carbon are tetrahedrally bonded diamond with a density of 3.5 g/cm^3, and the layered graphite structure with density of 2.4 g/cm^3. "Amorphous" carbon has been produced by a number of different methods that give rise to optically and electrically isotropic solids with densities ranging from that of "glassy carbon" (ρ = 1.47 g/cm^3) to evaporated films with reported densities from 1.35 to 2.4 g/cm^3. The short range bonding is thought to be similar to graphite, though some workers[18] have claimed that a significant amount of tetrahedral bonding is present. The large range of densities is probably produced by the presence of submicroscopic voids with dimensions $\lesssim$ 10 Å which are not readily detected with available imaging techniques. In any case, apparently uniform films as thin as 20 angstroms can be produced by arc evaporation onto smooth substrates.[19] We have been able to mount self-supporting films as thin as 81 angstroms.

Numerous studies of the optical and electrical properties of amorphous carbon have been reported.[20] The optical properties of glassy carbon have been measured,[21] and its dielectric function is well established for energies up to 82 eV.[22] The results vary, however, with the density.[23-25] Since amorphous carbon has a range of values depending on the preparation conditions for the film, great care must be exercised in comparing new data to previously reported

results. Since the film density is needed in determining the attenuation length, a procedure determining density is described later.

CHAPTER III

EXPERIMENTAL APPARATUS

In the course of the experiment, three systems were needed. It was first necessary to devise a method for producing thin carbon films. A commercial carbon-arc evaporator was used for this purpose. Second, a means of measuring electron transmission through these films was needed. An ultrahigh vacuum system containing an electron gun, the samples, and a detector was designed for this purpose. Finally, since the attenuation length of amorphous carbon is highly dependent upon its density, a means of determining the density of the carbon film was needed.

Carbon Evaporator

Our films were prepared by vacuum evaporation in a commercial Mikros evaporator in which carbon is evaporated by an incipient arc drawn between two graphite rods. The evaporator was designed with a high current, low voltage circuit between two terminals holding the graphite rods. Vacuum evaporation was used in preference to other available methods because it produces uniform films of high purity whose thickness is relatively easy to control.

Experimental Chamber

The electron transmission experiments were performed in a stainless steel vacuum chamber containing an electron gun, a sample holder for the carbon films, and an electron energy analyzer and

collector. Copper gasket seals were used throughout the system. All experimental components (sample holder, electron detection box, high voltage feedthrough, etc.) except the electron gun were mounted on the top flange to facilitate beam alignment.

A mu-metal shield in the shape of a capped cylinder was installed in the vacuum chamber to reduce magnetic fields in the sample region. Holes were cut in the shield for the electron gun and sample manipulation, and for an observation window. Cylindrical mu-metal shields were also installed around the electron guns. The chamber shield served the additional function of shielding the sample region from charged particles produced in the ion pump attached directly to the chamber.

Three pumps were used to pump the system. An oil-free carbon-vane mechanical pump (ITT Model SYCGH20-1) was used for the initial pumpdown followed by two sorption pumps (Huntington Model EV-150), and a 60 liter per second ion pump (Varian Model 911-5034). During initial pumpdown with the mechanical pump, a control valve between the pump and the chamber was used to maintain a slow pumping rate that would not rupture the very thin carbon films. Asbestos heater tapes were wrapped around the exterior of the chamber to enhance the pumpdown rate. When the pressure was sufficiently low to turn on the ion pump, the control valve was closed and the system reached a pressure of 1×10^{-8} torr in one day. During data taking with the electron gun warm, the pressure increased to $2\text{-}5 \times 10^{-8}$ torr.

Two electron guns were used in the experiment. Schematic diagrams of each are shown in Figure 2. The high energy gun was a

ORNL-DWG 82-18734

HIGH ENERGY ELECTRON GUN

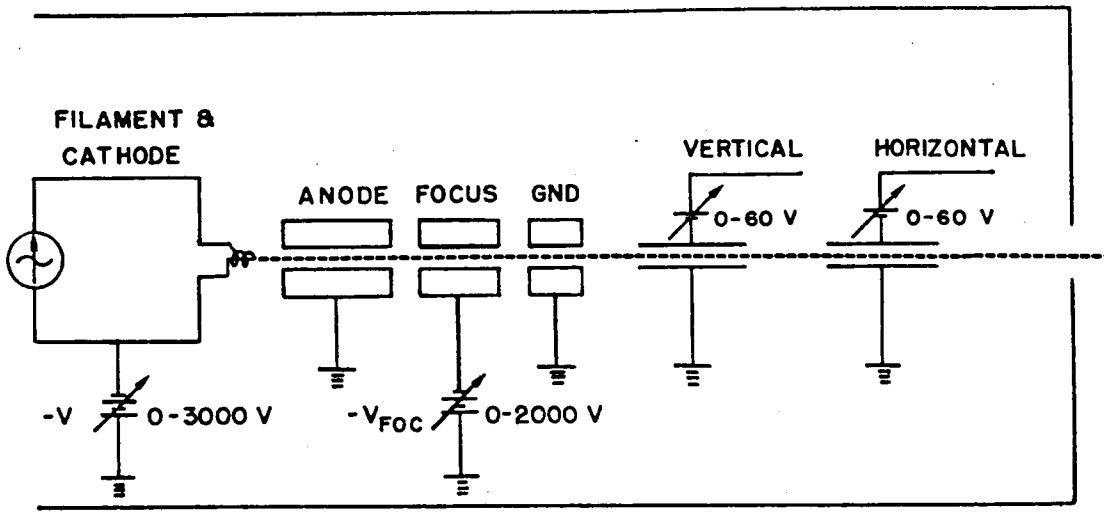

LOW ENERGY ELECTRON GUN

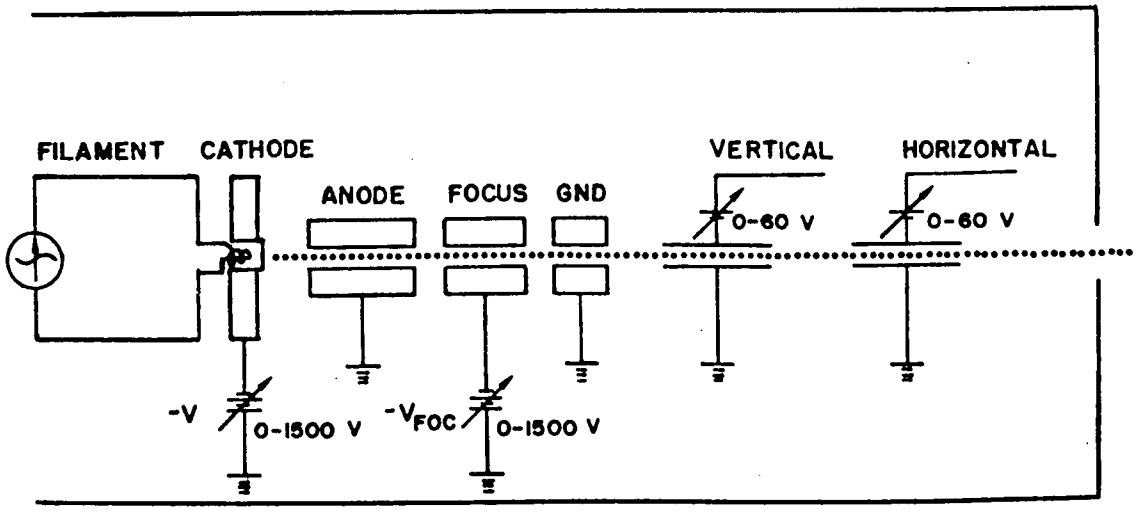

Figure 2. Circuit diagrams of the high and low energy electron guns and their power supplies.

commercial unit with a directly heated cathode and horizontal and vertical deflection plates. AC filament power and deflection voltages to ± 60 volts were supplied by a Varian Auger power supply. It was designed to allow AC filament voltage to float on a DC accelerating potential. A Fluke 415-B power supply with a range of 0 to -3000 volts provided the accelerating potential. Focus voltage was supplied by a PAR 280 high voltage supply. When focused, the electron beam had a cross-sectional area of a few square millimeters. Deflection plates were used to position the electron beam on selected regions of the sample surface. During the experiment, the deflection voltages differed only slightly from zero which indicated good equipment alignment. This gun was designed for electron energies between 500-3000 eV but could be used with sharply decreasing beam currents to 100 eV.

The low energy gun differed from the high energy gun by having a large, indirectly heated cathode and shorter focusing electrodes. The cathode was set at the accelerating potential, and was heated by a filament positioned closely behind it. Its 1/8-inch diameter emitting button produced a focal spot of 10 square millimeters or greater. An ORNL built power supply provided the AC filament voltage for this gun. Accelerating voltages were provided by a Kepco ABC-1500M supply. Deflection plates were mounted on the gun for beam manipulation, and powered by the same Varian supply used for the high energy gun. This gun operated most satisfactorily between 200 and 600 eV, but was used successfully between 50 and 1500 eV. Below 200 eV the beam current decreased rapidly, and above 600 eV the beam focus became poorer. For most films data were taken with both guns over their full available

range. The large region of overlap (200 to 1500 eV) provided a check on the consistency of the data.

The sample holder had positions for mounting three samples in a vertical array. The insulated holder was positioned in the experimental chamber by a metal bellows sealed manipulator that allowed approximately three inches of vertical motion and full rotation of the sample. The vertical motion allowed each of the three sample positions to be placed between the gun and the detector. A hole was placed at the bottom of the sample holder to observe the unattenuated beam current from the electron gun. In most experiments carbon films were placed in two of the sample positions, and a sample mounting plate with supporting screen, but without a film, was placed in the third position and used for measuring the incident flux.

As will be described later, the thin carbon films were supported on wire mesh spanning 3/8-inch diameter holes in the sample mounting plate. Hole-free uniform films of sufficient size to cover the 3/8-inch hole were seldom obtained however. Electrons passing through defects in the film could easily exceed the attenuated beam that had passed through the film. To avoid this problem, a masking plate with a 2.5-millimeter diameter hole was placed over a uniform, hole-free segment of the mounted film. Identical masks were placed on both the sample and empty support-screen positions. This masking procedure had the desirable side effect of allowing us to obtain accurate transmission measurements even with the large focal spot of the low energy electron gun. Once the desired intensity of the incident flux was chosen, the mounting assembly was kept perpendicular to the electron beam.

Electron Detection System

An electron detector was designed to measure the electron current being transmitted through the carbon films. The detector basically consisted of an electron collector cup mounted inside a grounded box behind a retarding potential screen as shown in Figure 3.

Electrons were collected after passing through a parallel plate retarding-potential energy-analyzer. The first plate of the energy-analyzer consisted on a 90 percent transparent stainless steel mesh screen spot-welded over a 1/4-inch hole in the grounded box. The retarding element was a second screen spaced about three millimeters behind the first that was spot-welded over a 3/8-inch hole in an electrically isolated plate. In most experiments the retarding potential was set at the negative accelerating potential plus ten volts by another 415-B Fluke power supply. Thus, only electrons with energies within 10 eV of the incident electron energy were passed to the collector.

Electrons were collected by a one centimeter diameter funnel of a channeltron maintained at ground potential and spaced about three millimeters behind the retarding screen. The channeltron was initially installed to allow measurement of very small beam currents using electron counting techniques. This capability was not used in our experiment. Instead, beam currents were measured directly using a Keithley 414 picoammeter. A Honeywell chart recorded the current measurements on chart paper.

ORNL-DWG. 82-19141

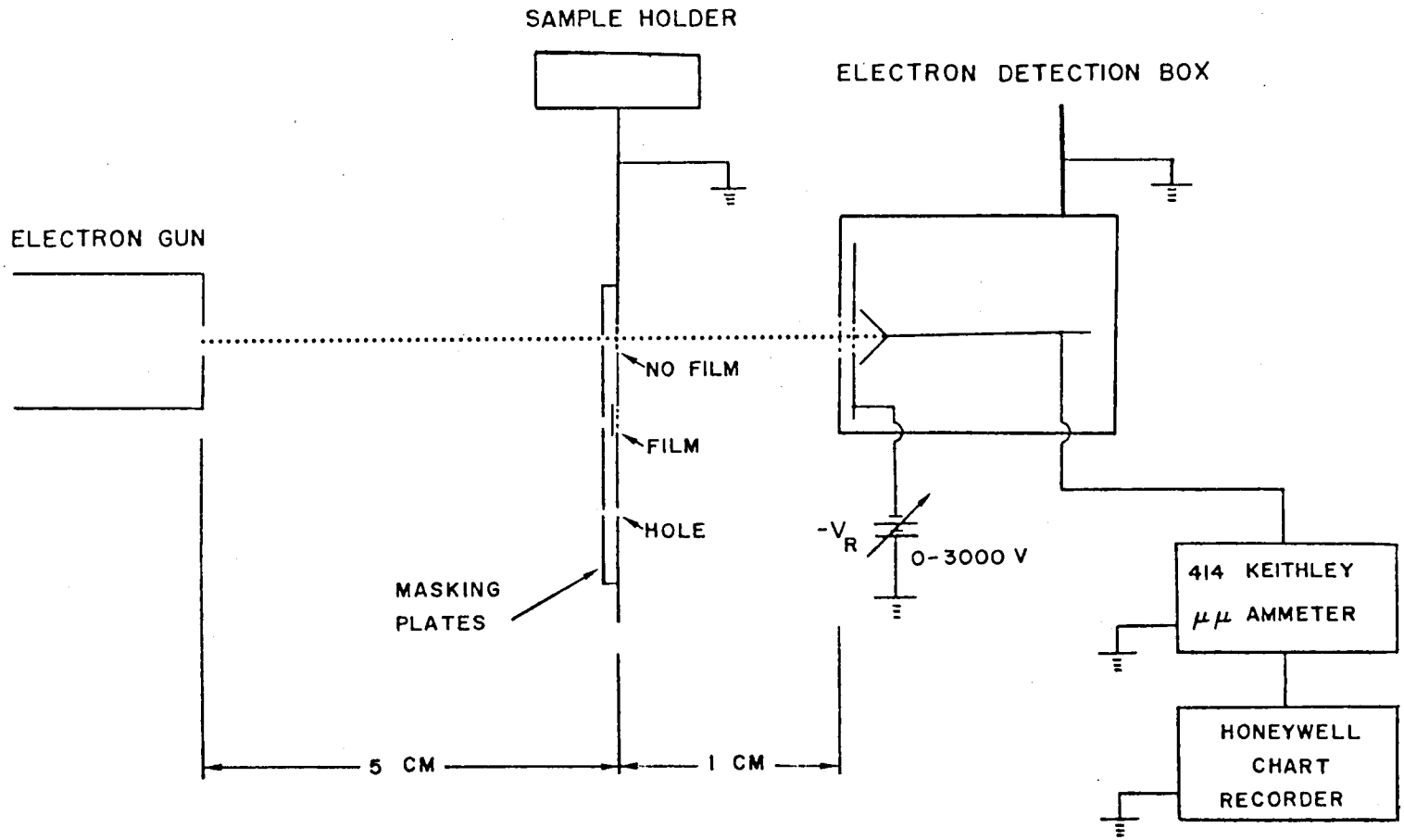

Figure 3. Schematic diagram of the experimental apparatus.

All electrical connections within the chamber were spot-welded with stainless steel wire. Ceramic insulated tubing was installed around the wire from the point of contact inside the grounded box to the high voltage BNC feedthroughs for electrical insulation. Exterior to the experimental chamber, all connections from the feedthroughs to the apparatus were made with BNC coaxial cables. The detection box was electrically grounded to the experimental chamber. A universal ground was therefore established for the components of the experimental chamber, the UHV system, and the equipment rack.

Film Thickness Monitor

The thickness of evaporated aluminum and carbon films was measured for programmed densities using an XMS-3 Inficon quartz crystal thickness monitor. The instrument operates on the principle that the frequency of a vibrating quartz crystal is dependent upon its mass. Therefore, evaporating matter onto the crystal changes its mass (and hence frequency) and allows one to determine the thickness. A glass slide for collecting the carbon film and the quartz crystal were placed in the evaporation chamber equidistant from the carbon or aluminum source. They were positioned so that both were coated with the same thickness of the evaporated material. Since carbon evaporates around 3000 degrees celsius and the quartz crystal frequency is sensitive to temperature, the crystal monitor was cooled with cold water pumped through copper tubing surrounding the crystal.

Angstrometer

To calibrate the thickness monitor, thicknesses of carbon and aluminum were measured using an M-100 Sloan Instruments angstrometer. In the angstrometer, light reflected from a highly reflecting weakly transmitting plate on the object lens of the instrument and from the surface of the film form interference fringes that are viewed through a low powered microscope. Sodium light of 5890 Å wavelength is used for illumination. The fringe to fringe distance corresponds to a vertical distance of $\frac{\lambda}{2}$ or 2945 Å. The film thickness in angstroms can be found by dividing the fringe shift across the film edge by the fringe to fringe distance, and multiplying by 2945 Å. Thicknesses of both carbon and aluminum were measured by this method.

CHAPTER IV

EXPERIMENTAL PROCEDURE

The experiment consisted basically of three parts: thin film preparation, electron transmission measurements, and determination of the density and thickness of amorphous carbon films. We describe here the procedure used to prepare the film, to measure the density, and to measure the electron transmission through them as a function of energy.

Sample Preparation

Clean glass slides were used as substrates for carbon evaporation. Initially, the slides were washed with Knox-60 laboratory glass cleaner, and then rinsed successively in hot tap water and cool distilled water. Finally, they were placed in ethyl alcohol, and allowed to dry in a contaminant free region. The same procedure was repeated if necessary.

A soap film was then applied to one side of the slide. The soap was obtained by grinding a portion of a bar of laboratory hand soap, pulverizing it with a mortal and pestle, and mixing the powder in distilled water. All containers and equipment used in this preparation were kept as contaminant free as possible.

The application of the soap film on the glass slides was an important part of the preparation. The soap film acted as an excellent parting agent[26] and provided a relatively flat surface for the evaporated carbon. It was necessary to apply the soap film evenly in

order to obtain smooth carbon films. Also, it was found that the soap film had to be thick in comparison with the carbon film in order to act as an efficient parting agent. Attempts were made to use a number of different materials as parting agents, but the hand soap mixture proved to work best when the films were floated off onto the water surface.

The Mikros vacuum evaporator was used to evaporate thin carbon films onto the soap surface. Two high purity (0.999) carbon rods were installed in the system's vacuum chamber as electrodes; after the system was under vacuum, an arc was struck which heated one electrode tip to approximately 3000 degrees Celsius. One rod was honed to a thin cylindrical shape with a lathe so that a white hot glow appeared at the point of contact. Glass slides coated with the soap film were placed around the perimeter of the bell jar vacuum chamber so that all points of their surface area were equidistant from the point source. Evaporated carbon was deposited onto the slides at a rate of about 5 angstroms per second. Typical evaporation times were 10 to 30 seconds. The pressure in the bell jar had to be low enough to allow evaporation, but it was not a crucial part of the film preparation. The total time for the production of the glass-soap-carbon sandwich including pumpup and pumpdown was approximately two hours.

Next, the carbon film was separated from the glass slide by floating the carbon film off the slide onto a pool of cool distilled water. The soap acted as parting agent which dissolved easily as the slide was slowly immersed into the water.

The art of making thin contaminant-free films was difficult to acquire. Care had to be taken in removing the carbon film from the slide slowly so that no rips and tears were created in the film's surface. Initially, the edges of the glass slide were scraped so that the film would begin its separation easily. Cool distilled water was used so that the surface tension of the water was suitable for float off. Warm water was not as desirable because breaks and tears in the carbon film were more prominent. Distilled water was used instead of tap water to prevent suspended particulate matter from collecting on the films as they were dried. With practice, continuous segments of carbon film could be obtained. Exclusive of any thickness measurements, the relative magnitude of the thicknesses of the films could be estimated by simply observing the shade of the films on the surface of the water. Upon completion of this step, the films were ready to be picked up from the surface of the water.

In order to obtain continuous segments of carbon films for study, the films were supported on 829-line-per-inch Ni mesh with 45% optical transparency. The mesh was affixed to stainless steel mounting plates using conductive silver paste and baked at 230 degrees Celsius in an oven. The carbon films were then slowly lifted from the surface of the water onto the wire mesh mount, and placed in a near vertical position to dry. Dried films were examined by an optical microscope to find continuous segments not containing visible holes. When a continuous segment was found, a masking plate with a 2.5 millimeter hole was placed over this segment, and the assembly was mounted onto a sample holder for later study. Additionally, an identical masking

plate was placed over a mounting plate with wire mesh but containing no film, and this assembly was also mounted onto the sample holder to be used for measuring the incident electron intensities, I_o. Since electrons can easily be transmitted through holes too small to be resolved optically, each film was examined to be sure that electron transmission became unmeasurable at low energies.

Optical Transmission Measurements

Before installing the films into the experimental chamber for electron transmission measurements, the thicknesses of the films had to be determined optically. Transmission measurements were made using a Spectra Physics Model 134 helium-neon laser (6328 Å) with an NRC Model 82 optical detector, and a Spectra Physics Model 166 argon ion laser (5145 Å). For our thinner films, the difference in optical transmission at these two wavelengths was negligible. The laser beam was positioned so that the beam passed through the masked areas. The incident intensity, I_o, of the laser beam passing through the wire mesh containing no film, and the transmitted intensity, I, of the beam passing through the mesh containing film were then measured. The background intensity, I_{bg}, was also measured by blocking the laser beam. The optical transmission through the film was determined by computing

$$\frac{I - I_{bg}}{I_o - I_{bg}} . \qquad (32)$$

From the optical transmission, the thickness of each carbon film was

determined from a curve of carbon film thickness vs. optical transmission shown in Figure 4.

Since thin films often do not have the same optical properties as bulk materials, and since the optical constants of carbon are known to vary with density and preparation procedure, we could not simply measure the bulk optical constants of thick films and use them to determine a calibration curve. Also, no direct means was available for accurately determining thicknesses of films $\lesssim$ 100 Å thickness. Consequently, the following two-step procedure was used to obtain the data points in the calibration curve.

A series of stepped films were prepared on glass slides, with each slide containing several film segments with thicknesses ranging upward from 10 Å, and at least one segment with 300 to 500 Å thickness. The relative thicknesses of the film segments on each slide were determined using a quartz crystal monitor, assuming that the film thickness was directly proportional to the measured surface density of the deposited film. The absolute thickness of the thickest film on each slide was then measured using an interferometer to provide an absolute calibration of all of the films on that slide. The scatter in the data points reflects primary uncertainties in the thickness measurements, which we estimate to be ±25%. There may also be some real variation in film density that contributes to scatter, but other experiments described below indicate that density varied less than 5% using our evaporation technique.

Interferometric thickness measurements were performed as follows. The silver coated slides of both aluminum and carbon were examined for

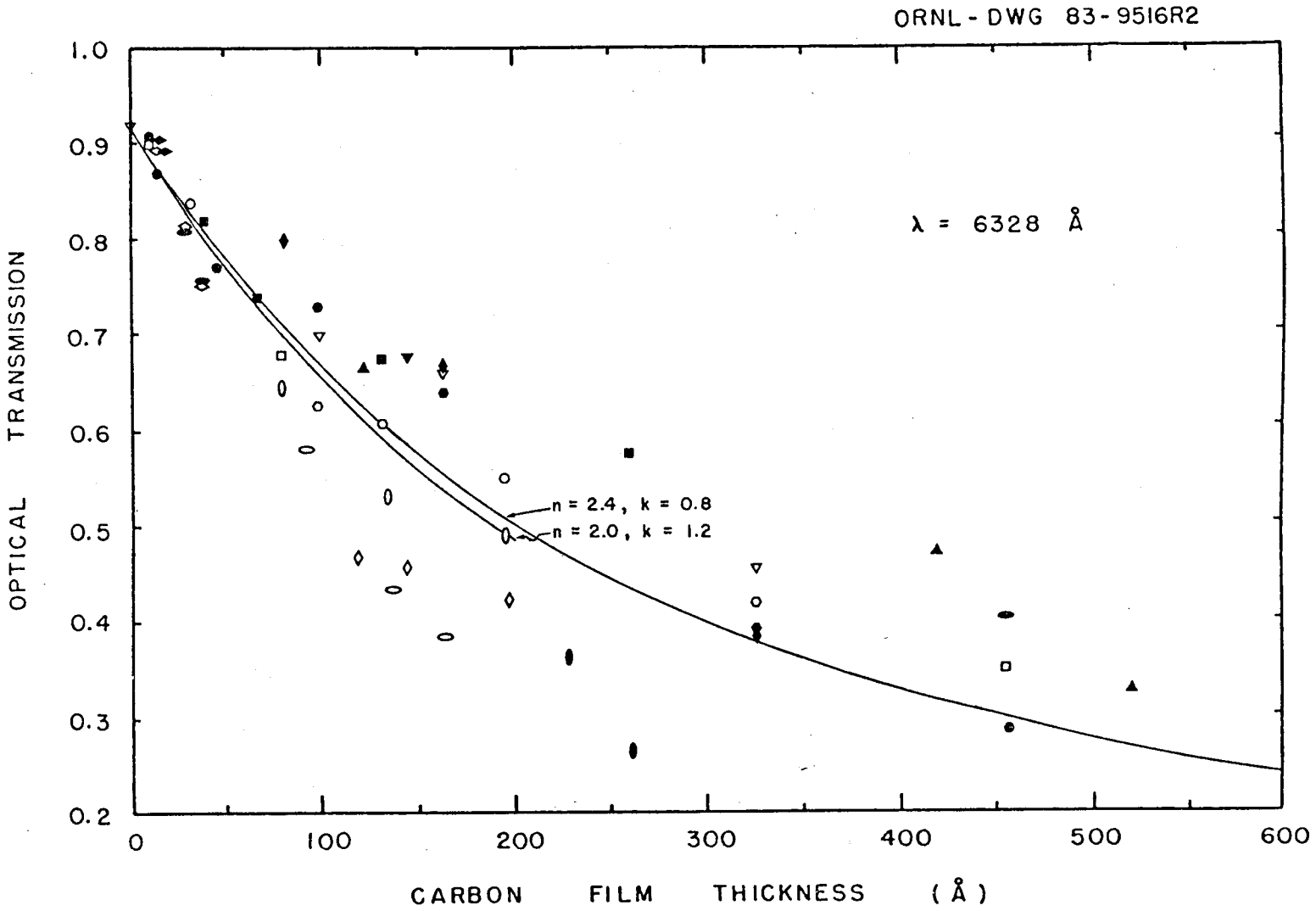

Figure 4. Carbon film thickness on glass vs. optical transmission. The wavelength of light was 6328 angstroms.

interference fringes and step-heights, and photographed for later study. Step-heights were recorded at several intervals across the slide. The maximum thickness on the glass slide corresponds to the thickness collected by the quartz crystal in the film thickness monitor. Using this procedure, the thickness of each carbon film under study was established.

Density Determination of Amorphous Carbon

The determination of the density of the carbon films was necessary for the proper interpretation of the electron transmission data. Initial attempts to determine the density used a quartz crystal thickness monitor to determine the surface mass density (g/cm^2) of the carbon film. The film thickness was then measured using an optical interferometer. The film's volume mass density is then determined by dividing the surface density by the film thickness. Values of the density obtained in this way were $\rho = 2.0 \pm 0.3$ g/cm^3. As noted above, however, the thickness measurements contain large errors which are directly propagated into the determination of the density. Consequently, another, more direct method of measuring the density was adopted.

The density of our samples was determined by submerging them in mixtures of carbon tetrachloride ($\rho = 1.594$ g/cm^3) and bromoform ($\rho = 2.889$ g/cm^3) mixed to give graded densities at 0.05 g/cm^3 intervals. These compounds were chosen because they have similar bonding structures and infinite solubility. Capped test tubes containing the mixtures were immersed in a constant temperature bath at room temperature. Fragments of films with varying thicknesses were placed

in the mixtures and were allowed to settle for two days. The fragments were seen to float in denser mixtures, and sank in lighter mixtures. From this, a density for any film thickness could be directly evaluated. For thicknesses between 100 and 1000 Å, our result for the density of our amorphous carbon films was 1.90 ± 0.05 g/cm^3.

Electron Transmission Procedure

In preparation for the electron transmission experiments, the experimental chamber had to be prepared for ultrahigh vacuum operating conditions. The chamber was first cleaned with distilled water and ethyl alcohol. A mu-metal can was then installed to reduce external magnetic fields. The electron gun, mounting plate, cover plate, and flanges were installed with copper O-ring gaskets. And finally, vacuum pumps and heater tapes exterior to the chamber were connected. The system was then ready for the UHV pumpdown procedure described in the previous chapter.

The mu-metal can was constructed to totally surround the contents of the experimental chamber. This reduced the magnetic field inside of the chamber threefold from 0.9×10^{-4} Tesla to 0.3×10^{-4} Tesla. A simple calculation of the radius of curvature for charged particles in a magnetic field, B, gives $r = 3.405 \frac{\sqrt{E}}{B}$ cm, where E is the incident electron energy in eV and B is the magnetic field in Tesla. It is noted that for the low energy E = 100 eV, and B = 0.3×10^{-4} Tesla that r = 113.5 cm which produces a total displacement of approximately 7 millimeters at the sample. This is easily correctable using the electron gun's deflection plates. Without the mu-metal can, the radius of curvature

of the electron would be decreased threefold, and the subsequent electron beam displacement would be noticeable.

For the electron transmission studies, low energy electrons emitted from the electron gun were focused on the carbon film surface, and transmission was measured by an electron detector in the form of current. The following procedure was used to measure these currents:

1. After the UHV system reached an operating value, the electron gun was turned on and allowed to warm up for ten minutes.

2. An accelerating potential and corresponding retarding potential were chosen. The retarding potential was set at ten volts less than the electron accelerating potential, except for the 125 Å film, which had a retarding potential which lagged the accelerating potential by 50 volts.

3. A focus voltage was chosen so that the width of the electron beam focused onto the carbon film mount was a minimum. The focus voltage for each accelerating potential remained fixed for electron transmission measurements through the film and through the supporting grid without film.

4. The gun emission was adjusted so that the transmitted current passing through the no-film hole, I_o, was approximately one microampere in the middle energy region ($\sim$1500 eV). For our thin films, this current was high enough to observe transmission through the films at low energies.

5. Upon obtaining the desired electron beam intensity, the beam was positioned to the masking holes by horizontal and vertical deflection voltages. When the equipment was properly aligned, these deflection voltages were small.

6. The sample holder was positioned to measure I_0, the current through the screened mesh, and then repositioned to measure I, the current through the film. Since the masking plates were in a vertical array, only vertical adjustment of the sample holder was required.

7. A background current, I_{bg}, was measured by positioning the sample holder so that no current from the electron gun was allowed to pass through the masking plate holes. Background current was measured on both sides of each hole.

The process was then repeated for the next electron energy. Transmission data were taken in 100 volt increments for energies between 100 to 3000 eV for each film. Only through the thinnest film was a small measurement above background obtainable at 50 eV.

CHAPTER V

RESULTS AND DISCUSSION

The data taken in this research were obtained by making thin continuous amorphous carbon films and by performing an electron transmission experiment through them. In order to interpret the data, the density and thickness of the films must also be measured. By the straightforward method described earlier, the density of our amorphous carbon films was found to be 1.90 ± 0.05 g/cm^3. Before going to the discussion of the transmission data, then, the experimentally determined film thicknesses are discussed briefly.

Thickness Determination

Film thickness and electron transmission are the two parameters needed for the direct calculation of the attenuation length. The thickness was determined by measuring the optical transmission of 6328 Å light through each of the samples, and comparing it to the optical transmission versus film thickness data shown in Figure 4. After making a correction for the transmission of light through glass, the thickness of our carbon films could be determined from the graph.

Data points in Figure 4 were acquired as described earlier. The solid lines in Figure 4 are theoretical optical transmission curves for a carbon film having a volume density of 1.90 g/cm^3 and complex refractive indices of $\hat{n} = (2.4 + i\ 0.8)$ and $\hat{n} = (2.0 + i\ 1.2)$. The former is the best least square fit to all of the data shown, and the latter is the best fit to the data points below 200 Å. The former

agrees very well with reported optical parameters of arc-evaporated carbon films (n = 2.4, k = 0.75). Both curves fit well within the scatter of the experimental points. Choosing the lower curve to represent the worst possible fit to the data for acceptable values of n and k, we found a ±8% uncertainty in the determination of our sample film thicknesses. This includes a ±2% error in measuring the optical transmission through our sample films.

The thicknesses of the four carbon films used in the study were determined from the upper calibration curve of Figure 4 to be 81 Å, 116 Å, 125 Å, and 210 Å with estimated errors of ±8%.

Determination of Electron Attenuation Length

An attenuation length was determined for each electron energy in the following manner. Incident (I_o) and transmitted (I) beams were measured as described earlier. A background current (I_{bg}) was also measured by positioning the sample holder to block the incident beam. The transmission was calculated as

$$T = \frac{I - I_{bg}}{I_o - I_{bg}} .$$

Since $T = e^{-t/L}$, where L is the attenuation length and t is the film thickness, the attenuation length is given by

$$L = -t/\ell nT . \qquad (33)$$

Figure 5 is a graph of the electron attenuation lengths calculated from the measured transmittance data for the four carbon films versus the electron energy. Between 50 and 3000 eV, the attenuation length increases smoothly from about 12 to 58 angstroms. The error bars

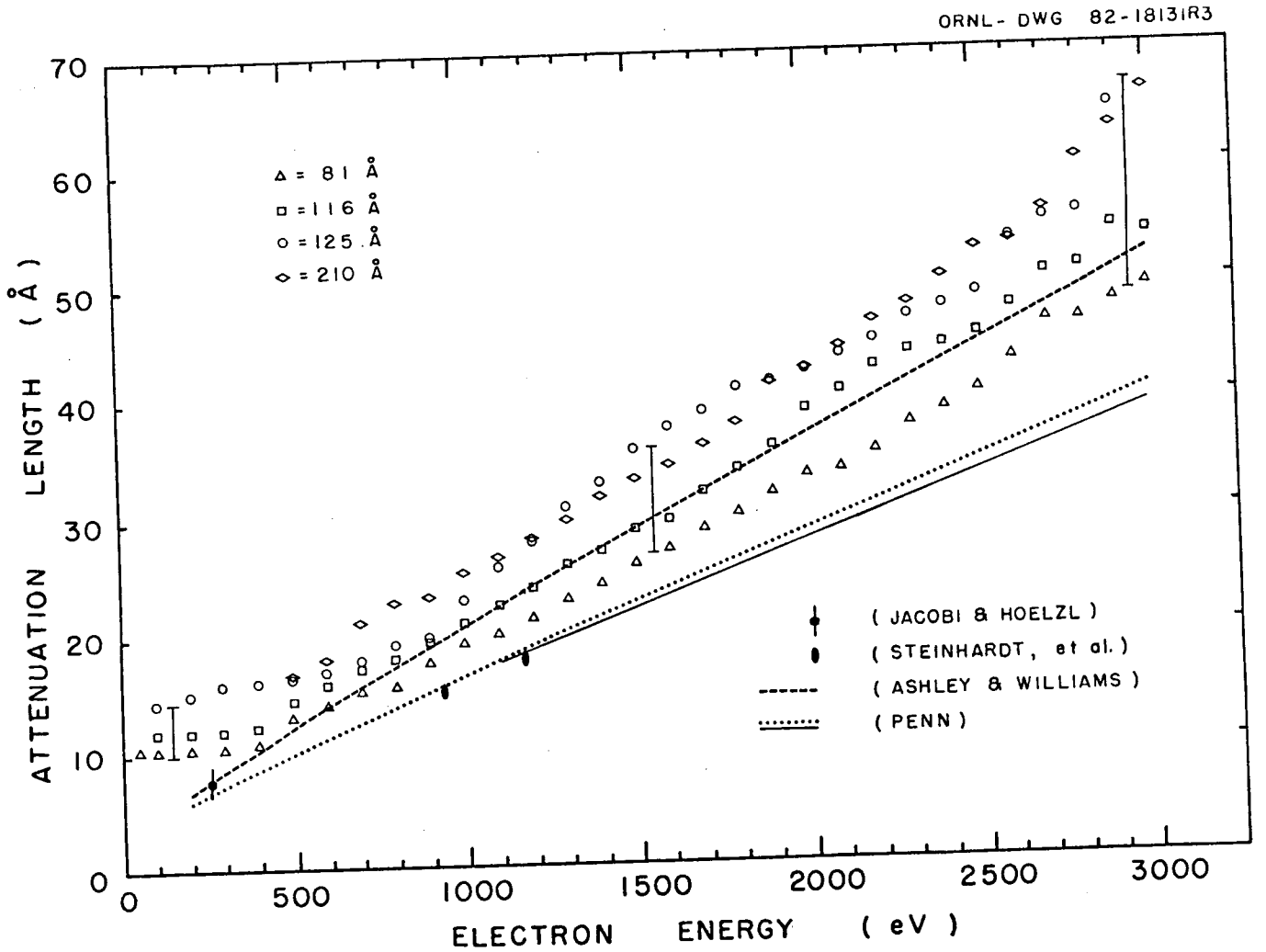

Figure 5. Electron attenuation length as a function of electron energy. The mean free path theories of Ashley and Penn are the dashed and dotted curves; the experimental data are shown as points.

result primarily from the ±8% uncertainty in the film thicknesses, and from a ±13% standard deviation scattering error. The dotted line is calculated from Penn's free-electron model using a carbon film density of 1.9 g/cm^3; it represents the mean free path due to valence electrons only. The solid line represents the mean free path when the core electron contribution has been added. The dashed line is calculated from Ashley and Williams' empirical equation for organic solids of the same density. Using optical constants of glassy carbon of density ρ = 1.47 g/cm^3 and scaling the results for larger electron densities,[27] Ashley has calculated a mean free path for carbon with density ρ = 1.9 g/cm^3 lying very close to the dashed line. Other experimental values of electron attenuation lengths for amorphous carbon shown in Figure 5 are (7.5 ± 1.5) Å at 263 eV from Jacobi and Hoelzl,[28] and 15 Å and 18 Å at 920 and 1169 eV, respectively, from Steinhardt et al.[29] No error limits were given for the latter values. Both assumed a density of 2.0 g/cm^3 in their calculations. Our data points between 500 and 3000 eV are in satisfactory agreement with Ashley and Williams' calculation of the mean free path if a density of 1.9 g/cm^3 is assumed.

We conclude that the observed electron energy losses cannot be described using a simple free electron model, but that they are most probably in good agreement with the losses that would be calculated from the energy loss function, Im $(\frac{-1}{\varepsilon})$ determined optically from values of ε_1 and ε_2 measured on films identical to those used in the transmission studies. In future experiments, we intend to measure the optical constants for our films so that a more exact comparison can be made.

A remark on experimental technique may be of value to future workers in electron transmission studies. Holes in the carbon films would introduce a serious error in the determination of the electron attenuation length. In the fabrication of the films, such holes could not be avoided, however they could be detected. In early efforts, supposedly good continuous film segments used in the electron penetration studies were found to have attenuation lengths that were rather flat over the energy region. Between 100 to 3000 eV, the attenuation lengths were found to range between 10 to 20 angstroms. Such flat curves over the wide energy region was a direct indication of the existence of microholes in the film. Optical transmission measurements failed to detect these adequately. We found that a quick check of the transmission data at high, medium, and low energies would provide an indication of whether the film under study had microholes.

In the study, the thinnest film (81 Å) had a transmitted current cutoff at 50 eV, and the thickest film (210 Å) had no measureable transmission at 500 eV. No data exist below these respective cutoff energies. This is also the best check for microholes; a small transmitted leakage current through the film at energies below the normal cutoff energy indicated the existence of microholes in the film.

This points out a basic constraint on the experiment. The thickness of a continuous film determines how low in energy one can go to observe electron transmission, i.e., the thinner the film, the lower the transmission energy cutoff, and the more one can learn about the low energy portion of the curve. If thinner films can be made, they will provide more information about the low energy region.

In the low energy range below 500 eV, we find a "flatter" curve than is predicted by theory. That is, the mean free path is larger and increases more slowly with energy than theory predicts. Qualitatively, more electrons are being collected. The effect is not due to microholes in the film because this would produce a curve of different shape. The increased ratio of elastic to inelastic scattering expected at low energies cannot be responsible because anomolously lower, rather than higher mean free paths would be produced. At low energies it is more difficult to separate scattered and unscattered electrons so that perhaps the capture of scattered electrons can enhance the measured mean free path. Nevertheless, future experiments are planned, using an improved energy analyzer in which full energy distribution will be measured at low electron energies. Using this data, it should be possible to accurately separate elastic and inelastic electrons, so that a better measure of inelastic mean free paths can be obtained at lower energies.

In this research, low energy electron transmission of thin amorphous carbon films was investigated. The electron attenuation length was found to be 12 to 58 angstroms over the energy range of 50 to 3000 eV. The density of amorphous carbon was found to be 1.90 ± 0.05 g/cm^3 and the four film thicknesses, 81 Å, 116 Å, 125 Å, and 210 Å, used in the study were determined from optical transmission data of arc-evaporated carbon on glass. Over the energy range between 500 and 3000 eV, the data agree well with the theoretical calculations using values of $\mathrm{Im}\left(-\frac{1}{\varepsilon}\right)$ determined from optical data.

The most difficult task in the research was the manufacture of hole-free thin carbon films. An experimental method for checking films for microholes was established.

The major parameter limiting the accuracy of the measured mean free path was the thickness of the amorphous carbon films. The error bars in Figure 5 indicate the systematic error in the determination of the thickness and scattering in the electron transmission data.

Data were not obtainable below 50 eV as electron transmission was not measurable below this energy for the thinnest film used in the study. A method of preparing thinner continuous films must be developed if transmission measurements are to be extended below 50 eV.

BIBLIOGRAPHY

BIBLIOGRAPHY

1. E. Rudberg, Proc. Roy. Soc. (London) A127, 111 (1930).
2. G. Ruthemann, Naturwissenschaften, 9, 648 (1941).
3. M. P. Seah and W. A. Dench, Surf. Interface Anal., 1, 2 (1974).
4. D. Bohm and D. Pines, Phys. Rev. 82, 625 (1951).
5. R. H. Ritchie, Phys. Rev. 106, 874 (1957).
6. E. A. Stern and R. A. Ferrell, Phys. Rev. 120, 130 (1960).
7. J. J. Quinn, Phys. Rev. 126, 1453 (1962).
8. A. W. Blackstock, R. H. Ritchie, and R. D. Birkhoff, Phys. Rev. 100, 1078 (1955).
9. G. W. Jull, Proc. Roy. Soc. B69, 1237 (1956).
10. J. R. Crowell, W. G. Spitzer, L. E. Howarth, and E. E. Lebate, Phys. Rev. 127, 2006 (1962).
11. R. W. Soshea and R. C. Lucas, Phys. Rev. 138, 1182 (1965).
12. F. W. Garber, M. Y, Nakae, J. A. Harter, and R. D. Birkhoff, J. Appl. Phys. 42, 1149 (1971).
13. P. L. Walker and P. A. Thrower, eds, Chemistry and Physics of Carbon, Vol. 11 (Marcel Dekker, Inc., New York, 1973), p. 248.
14. I. Landau and W. E. Spicer, J. Elec. Spectros. Relat. Phenom. 3, 409 (1974); C. J. Powell, Surf. Sci. 44, 29 (1974).
15. J. Lindhard, K., Dan. Vidensk. Selsk., Mat.-Fys. Medd., 28 (8), 1-57 (1954).
16. D. R. Penn, J. Electron Spectrosc. Relat. Phenom. 9, 29 (1976).
17. J. C. Ashley and M. W. Williams, Radiat. Res. 81, 364 (1980).
18. J. Kakinoki, Acta Cryst. 13, 171, 448 (1960).
19. M. L. A. Vicar, J. Appl. Phys. 41, 4765 (1970).
20. L. B. Leder and J. A. Suddeth, J. Appl. Phys. 31, 1422 (1960).

21. E. A. Taft and H. R. Philipp, Phys. Rev. 138, A197 (1965).

22. E. T. Arakawa and M. W. Williams, J. Appl. Phys. 43, 3460 (1972).

23. D. E. Palin, Nature 178, 809 (1956).

24. W. Langbein, Naturwissenschaften 45, 510 (1958).

25. E. F. Kennedy and D. H. Youngblood, Phys. Rev. 158, 897 (1967).

26. E. T. Arakawa, M. S. Chung, and M. W. Williams, Rev. Sci. Instrum. 48, 707 (1977).

27. E. T. Arakawa, M. W. Williams, and T. Inagaki, J. Appl. Phys. 48, 3176 (1977).

28. K. Jacobi and J. Hoelzl, Surf. Sci. 26, 1016 (1971), and the detailed study of K. Jacobi, "Elektronenspektroskopie dunner Kohlenstoff-folien in Reflexion and Transmission," Thesis, Technische Universitat, Claustal, Germany, 1970.

29. R. G. Steinhardt, J. Hudis, and M. L. Perlman, Phys. Rev. B5, 1016 (1972).

VITA

Charles Martin was born in Asheville, North Carolina, on May 13, 1951. He attended elementary schools in Oak Ridge, Tennessee, and was graduated from Oak Ridge High School in June 1969. In the summer of that year he entered The University of Tennessee, Knoxville, and in December 1976 he received a Bachelor of Science degree in Engineering Physics. During the period between 1974 and 1976 he worked with the Tennessee Valley Authority as an engineering cooperative student. In the winter of 1977 he began study toward a Master's degree in physics at The University of Tennessee while remaining professionally employed. In the fall of 1980 he accepted a research assistantship with the University and received the Master of Science degree in August 1983.

The author is a member of Sigma Pi Sigma Society of Physics Students, the American Physical Society, and the United States Chess Federation. He plans on continuing his graduate research studies at The University of Tennessee, Knoxville.